Prediction of Turbulent Heat Transfer and Pressure on Swept Leading Edges

HUGH W. COLEMAN* AND E. CLARK LEMMON*
Sandia Laboratories, Livermore, Calif.

As a result of an extensive experimental study, a technique has been developed for predicting shock shapes, pressures, and turbulent heat-transfer rates on the leading edge of a fin, swept wing, antenna, or similar highly swept protuberance near its intersection with a high-velocity vehicle. Comparison of predictions with data of the present experiment and those of others indicates good agreement. While pressures in the intersection region are higher than infinite swept cylinder theory predictions, heat-transfer rates can be either significantly greater or less than values predicted by this theory depending on local flow conditions and geometry.

Nomenclature

D = leading-edge diameter
h = heat-transfer coefficient
M = Mach number
P = pressure
Pr = Prandtl number
Re = Reynolds number
R_N = nose radius
S = distance up the leading edge
T = temperature
u = velocity
Z = distance normal to body surface
δ = boundary-layer thickness
Δ = dimensionless pressure increase
Λ = leading-edge sweep angle
ϕ = circumferential angle on cone
η_r = recovery factor

Subscripts
c = compressible
e = boundary-layer edge at position 1
es = effective sweep
I = incompressible
o = total conditions
rec = recovery conditions
s = stagnation line
t = turbulent
ICT = turbulent swept infinite cylinder theory of Ref. 1
w = wall conditions
x = surface distance along cone
∞ = tunnel freestream conditions
1 = conditions just upstream of leading-edge shock

Introduction

CONTROL fins used on high-velocity vehicles are subjected to severe aerodynamic heating and high pressures. Therefore, the fins are typically highly swept with a cylindrical leading edge and may be only a few boundary-layer thicknesses high. The case in which the flowfield around the fins is turbulent is of particular interest because of the high heating rates. Analytical approaches such as the turbulent theory of Beckwith and Gallagher[1] for swept infinite cylinders are available for analysis of such configurations. However, the complexities of the flow interference near the intersection of the fins and the vehicle place the prediction of pressure and heat transfer on the leading edge of the fin beyond the scope of such methods. Some empirically-based modifications are necessary.

References 2–4 present pressure and heat-transfer data on highly swept cylindrical leading edges in unseparated turbulent flow. Reference 2 includes data from a 60° swept cylinder mounted on an 8° half-angle wedge at a freestream Mach number of 4.15. Similarly, Ref. 3 presents data from a 60° swept cylinder mounted on a 12° half-angle wedge at a freestream Mach number of 8. In both cases, the data within the influence of the wedge flow are above predictions for undisturbed flow on swept infinite cylinders. However, the authors obtained reasonable agreement with their data by using a modification of infinite cylinder theory based on the use of effective shock angles measured from schlieren photographs. Reference 4 includes data on a 70° swept leading edge immersed in a thick tunnel-wall boundary layer at Mach 6.15. The pressure data were above theoretical values near the root of the leading edge; however, present calculations show the heat-transfer data to be below that predicted by the methods of Ref. 1 in the root region.

The objective of the present investigation was to develop techniques for predicting turbulent heat transfer and pressures on vehicle control fins. The experimental program discussed below was undertaken to systematically obtain turbulent heat-transfer and pressure data on fins of various sweeps, heights, leading-edge diameters, and face shapes. The fins were mounted on a 6° half-angle cone. Two noses were used, one sharp and one 40% blunt, to cause different local flow conditions at the fins. Freestream Mach numbers ranged from 2.71–4.97 and freestream Reynolds numbers from 7.7×10^6/ft to 2.8×10^7/ft. Boundary-layer thicknesses were about $\frac{1}{3}$ to $\frac{1}{2}$ the fin height, and no evidence of separation was observed. A more detailed discussion of the results of the experimental investigation is presented in Refs. 5–7.

Test Program

Test Facility

The tests were conducted in the LTV Aerospace Corp.—Vought Aeronautics Div. High Speed Wind Tunnel. The facility is an unheated atmospheric exhaust, blow-down tunnel with a 4×4 ft test section. A detailed description of the facility is given in Ref. 8.

Model Description

The model was a 6° half-angle cone with interchangeable sharp and blunt ($R_N \doteq 2.0$ in.) noses. Four positions 90° apart

Presented as Paper 73-667 at the AIAA 6th Fluid and Plasma Dynamics Conference, Palm Springs, Calif., July 16–18, 1973; submitted July 16, 1973; revision received February 28, 1974. This work was supported by the U.S. Atomic Energy Commission, Contract AT-(29-1)-789.

Index categories: LV/M Aerodynamic Heating; Boundary Layers and Convective Heat Transfer—Turbulent.

* Member of the Technical Staff, Aerothermodynamics Division.

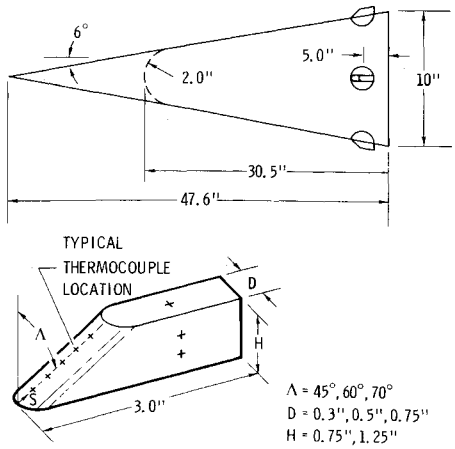

Fig. 1 Sketch of cone model and typical fin.

were available near the aft end of the model for mounting fins and disks (fin platforms) instrumented for pressure or heat-transfer measurements. Sketches of the cone and a typical fin are shown in Fig. 1. The cone body itself was instrumented with three thermocouples and one pressure port at the fin station and thermocouples fore and aft of one fin position. Provision was also made for mounting a pitot rake near the fin station for boundary-layer surveys.

Two fins and disks instrumented for pressure measurements were made of solid aluminum with 0.040 in. i.d. pressure ports, and the boundary-layer rake consisted of ten 0.020 in. i.d. tubes. Eleven heat-transfer fins were constructed of a phenolic core with a 0.018 in. thick Nickel-200 sheet overlay bonded with epoxy. Instrumentation consisted of iron-constantan thermocouples (0.008-in.-diam wire) welded to the nickel at prescribed locations. The various fin geometries included sweeps of 45°, 60°, and 70°; diameters of 0.30 in., 0.50 in., and 0.75 in.; heights of 0.75 in. and 1.25 in.; and several face shapes.

Test Procedures

For pressure runs, two fins instrumented with pressure ports were mounted at the $\phi = 0°$ and 180° fin positions and the pitot rake was mounted on the cone approximately at the fin station. Pressure measurements were made with two transducers connected to a pressure scanning switch. One transducer measured body and fin pressures and the other the rake pressures. The scan rate was 10 samples per sec.

Since the tunnel was unheated, the model was cooled using liquid nitrogen prior to the heat-transfer runs. A cover made of a foaming epoxy reinforced with fiberglass cloth was constructed in two halves and strapped on the model. The cover enclosed the model from the aft end up to the nose joint. Liquid nitrogen (LN_2) was then forced into the space between the cover

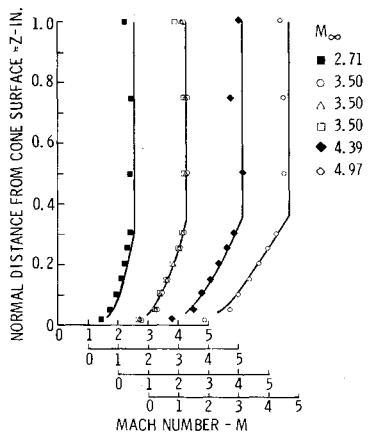

Fig. 2 Comparison of data and predicted Mach profiles for sharp cone runs.

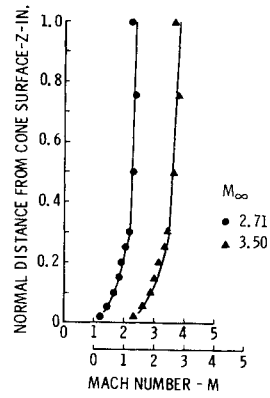

Fig. 3 Comparison of data and predicted Mach profiles for blunt cone runs.

and the model until the model was sufficiently cooled (typically to about −280°F). After cooldown was completed, the LN_2 fill apparatus was removed, the fill holes in the cover were plugged, and the test section was closed. When the desired tunnel test conditions were obtained, a solenoid switch was closed which simultaneously activated the data acquisition system, a burn wire which cut the straps on the cover, and two pneumatic pistons which pulled the cover halves apart using cables. Thermocouples were sampled 50 times each sec for 6 sec and the data stored on a digital computer. High-speed movies taken during a separation showed complete cover removal within 0.1 sec.

Spark shadowgraphs of the fin-cone interference region for the fins at $\phi = 0°$ and 180° were obtained during many of the pressure and heat-transfer runs. Real gas properties were used in the flow calculations for analysis of the data.

Data Reduction

Heat-transfer coefficients were determined from temperature data using a modification of the standard transient thin-skin technique, which assumes no temperature gradient normal to the skin surface. Since substantial conduction occurred in the spanwise and chordwise directions on the fin face due to variations in the heating rates and (to a lesser degree) initial temperature gradients, a technique was developed with the aid of numerical modeling of the thermal response of the fins to evaluate the resulting errors. In addition, the error caused by the presence of the thermocouple was experimentally determined. A detailed discussion of the data reduction technique and the evaluation of the sources of error is presented in Ref. 7. Accuracy of the heat-transfer data is estimated to be ±30%.

Discussion

Boundary-Layer Measurements

The variation of total pressure through the boundary layer was measured with the pitot rake during each pressure run, and the Mach number at each height was then determined using the static pressure measured on the cone at the rake location and normal shock relations. Figures 2 and 3 present the Mach profile data for the sharp- and blunt-cone runs, respectively. The upper two probes on the rake were bent and realigned in the tunnel during the course of the pressure runs, so the upper two data points in each profile are suspect. The Mach profile curves shown in the figures were calculated using the Crocco relation for unity Prandtl number

$$(T_o - T_w)/(T_{o,e} - T_w) = \frac{u}{u_e}$$

boundary-layer thicknesses estimated from the data, and a velocity variation of

$$\frac{u}{u_e} = \left(\frac{Z}{\delta}\right)^{1/n}$$

The exponents which best matched the data were $n = 10$ for the sharp-cone runs and $n = 7$ for the blunt-cone runs. This follows

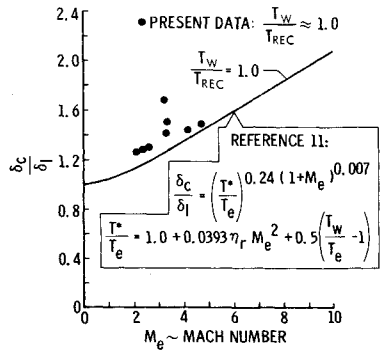

Fig. 4 Comparison of boundary-layer thickness data with compressibility correction of Eckstrom.[11]

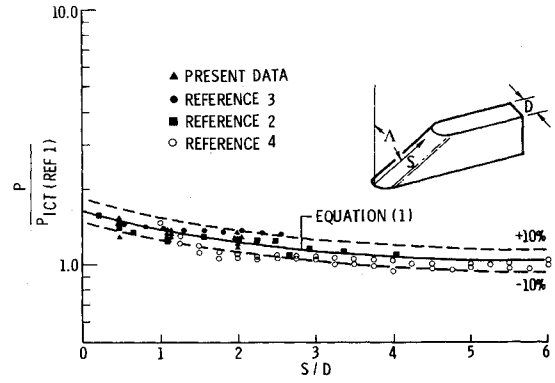

Fig. 6 Nondimensional leading-edge pressure data vs nondimensional distance up the leading edge.

the expected trend of an increasing n with increasing momentum thickness Reynolds number reported by others.[9]

Successful prediction of compressible boundary-layer thicknesses is necessary to obtain the upstream conditions required for analysis of control surfaces mounted on a vehicle. Compressibility corrections for boundary-layer thickness calculations have been suggested by several authors.[10,11] The present boundary-layer thickness data (δ_c) nondimensionalized by incompressible predictions (δ_I) are compared with the compressibility correction for turbulent boundary layers proposed by Eckstrom[11] in Fig. 4. Agreement is reasonable considering the accuracy with which δ_c can be estimated from the Mach profiles. The correction proposed by Martellucci[10] for a sharp cone at $M_\infty = 8$ agrees within a few percent with the prediction using Eckstrom's method.

Since no rake data were taken during the heating runs, boundary-layer thicknesses and property variations were calculated for analysis of the heat-transfer data. Location of transition was determined using a momentum thickness Reynolds number criterion. Eckstrom's compressibility correction was assumed valid and the Crocco relation was used for calculation of property variations through the boundary layer. The velocity profile exponent was taken as $n = 10$ for sharp-cone runs and $n = 7$ for blunt-cone runs. While the pressure data were obtained at $T_w/T_{rec} \approx 1.0$, the heat transfer data were taken at a ratio of approximately 0.35. This variation in temperature ratio resulted in different boundary-layer thicknesses for the heat-transfer and pressure runs for which tunnel freestream conditions were identical.

Pressure

For purposes of data analysis and comparison with turbulent infinite swept cylinder theory[1] (hereafter referred to as ICT), the boundary layer upstream of the fins was divided into several strips as shown in Fig. 5 with the local properties at a given X assumed constant across each strip. ICT values of pressure (and heat transfer) at a point on the fin leading edge were calculated using properties in a boundary-layer strip at the same geometric height.

Fin leading-edge pressure data nondimensionalized by local ICT values are shown in Fig. 6 vs nondimensional distance up the leading edge (S/D). The present data are compared with those of Beckwith[2] and Bushnell[3] taken on swept cylinders mounted on wedges and those of Bushnell and Jones[4] taken on a leading edge mounted on a tunnel wall. The present data are for $\Lambda = 60°$, $M_e = 2.16$–4.71, and $Re_{e,x} = 1.1$–8.3×10^7. The data of Ref. 2 were for a 60° swept cylinder mounted on an 8° half-angle wedge at a freestream Mach number of 4.15. The true geometrical sweep angle Λ of the cylinder was therefore 68° with respect to the wedge flow and the local Mach number was 3.56. Similarly, the data of Ref. 3 were for a 60° swept cylinder mounted on a 12° half-angle wedge at a freestream Mach number of 8, the geometrical sweep was 72° with respect to the wedge flow, and the local Mach number was 7.33. The wedge boundary-layer thickness in both cases was negligible. The data of Ref. 4 were for a 70° swept leading edge mounted in a thick tunnel wall boundary layer with a freestream Mach number of 4.15. The increase in pressure over ICT values at low S/D seen in Fig. 6 is caused by the deviation of the leading-edge shock from the parallel shock structure assumed in the theory, which results in a lower effective sweep angle. The deviation was observed by both Beckwith[2] and Bushnell[3] and was quite apparent in the current investigation.

A proposed correlation of the pressure data of the form

$$P/P_1 = (1.0 + 0.65\,e^{-0.55S/D})(P/P_1)_{ICT} \qquad (1)$$

is also shown in Fig. 6, where the subscript 1 indicates conditions just upstream of the fin shock and the ICT values were calculated using the strip method discussed above. The above expression provides a reasonable correlation of pressure data for $\Lambda = 60°$–$72°$, $M_e = 2.16$–7.33, and boundary-layer thicknesses which intersect the leading edge from $S/D = 0$–5.

Typical pressure data of the present investigation are compared with the predictions of Eq. (1) and theory[1] in Fig. 7. The "overshoot" predicted by the pressure correlation is a result of the combination of the S/D effect tending to increase the pressure as S/D decreases and the Mach number decreasing through the boundary layer.

The present pressure data nondimensionalized by local ICT pressures are shown in Fig. 8 vs the local upstream Mach number computed using the strip method The data indicate that,

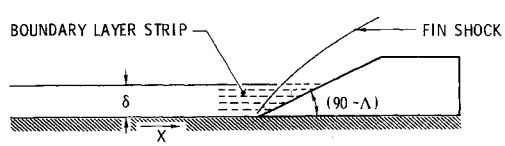

Fig. 5 Sketch of boundary-layer strip method.

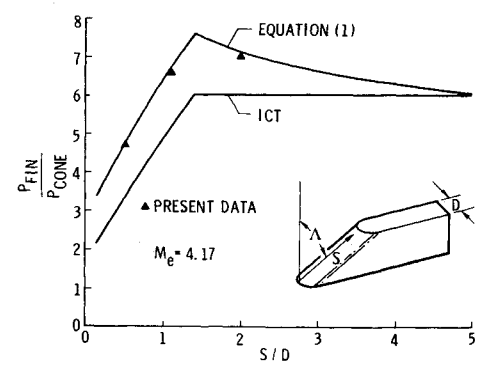

Fig. 7 Typical leading edge pressure distribution.

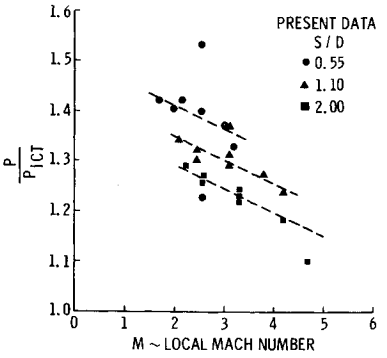

Fig. 8 Effect of local Mach number on leading edge pressure.

for a constant S/D, the pressure increase over ICT values decreases as the Mach number increases. This can possibly be explained by noting that shock standoff distance also decreases with increasing Mach number, therefore requiring less change in shock angle as the shock approaches the point of intersection of the leading edge and the body. However, the data of Refs. 2 and 3 do not fully verify the trend shown by the present data, and it was felt that the available data do not warrant inclusion of the observed Mach effect in the pressure correlation (Eq. 1).

A shadowgraph of the fin-cone interference region for one of the pressure runs is shown in Fig. 9. The deviation of the fin shock from a parallel structure is quite apparent. The shadowgraph also verifies that the flow was unseparated in the interaction region upstream of the fin. The shock shape predicted using Eq. (1) is also shown in the figure. The prediction assumed that the fin shock originated at the intersection of the fin and cone, and the strip method was used to determine the local sweep angle required for a parallel shock to provide the pressure rise calculated using Eq. (1). The good agreement between predicted and observed shock structure indicates that the pressure correlation can be used to provide reasonable estimates of shock shapes near the intersection of a leading edge and a body.

Heat Transfer

Heat-transfer measurements were obtained during 16 test runs on 11 different fins used in sets of four. Details of the fin-cone interaction region can be observed in the shadowgraphs of the 70° swept fin shown in Fig. 10. The sequence is arranged in order of increasing Mach and Reynolds numbers, and the trend of greater deviation of the fin shock from a parallel structure with lower Mach number is evident.

The fin leading-edge heat-transfer data of the present investigation are shown in Fig. 11 nondimensionalized by ICT values calculated using the boundary-layer strip method described above. The reference temperature used in the theory[1] was the temperature calculated for the edge of the boundary layer on an infinite cylinder at the geometrical fin sweep. It is obvious from this comparison that infinite swept cylinder theory underpredicts the present data.

Beckwith[2] and Bushnell[3] found that the heat-transfer data taken on swept cylinders mounted on wedges could be reasonably predicted by ICT using an effective sweep angle measured from schlieren photographs of the fin shock. This suggests that an effective sweep heat-transfer coefficient h_{es} can be calculated with ICT using the predicted shock angle as discussed in the previous

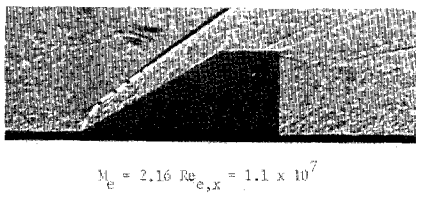

Fig. 9 Comparison of predicted and observed fin shock shapes.

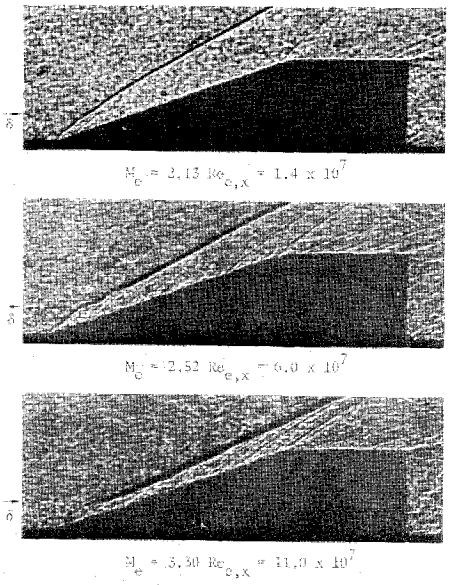

Fig. 10 Shadowgraphs of 70° swept fin for several flow conditions.

section and the pressure given by Eq. (1). However, the current results indicate that the variation of the turbulent stagnation line heat-transfer coefficient in the low S/D region ($\leqq 5$) can be represented by

$$h_{s,t} = k\left(\frac{P}{P_1}\right)^{1.52}$$

where P/P_1 is given by Eq. (1). If it is assumed that ICT values are reached at an S/D of 5 (independent of Mach number), then the constant k can be evaluated and the expression becomes

$$h_{s,t} = \left\{h_{\mathrm{ICT}}\left(\frac{P}{P_1}\right)^{-1.52}_{\text{Eq. (1)}}\right\}_{S/D=5}\left(\frac{P}{P_1}\right)^{1.52}_{\text{Eq. (1)}} \tag{2}$$

where the theoretical values comprising the constant are calculated using the strip method at $S/D = 5$ and the geometric sweep angle.

The heat-transfer data of Beckwith[2] and Bushnell[3] are compared with the predictions of the effective sweep method and Eq. (2) in Figs. 12a and 12b, respectively. The effective sweep method is generally below the data in both cases, while the present predictions match the data of Beckwith very well and give fair agreement with Bushnell's data. The wedge boundary layer in Refs. 2 and 3 was negligible, so the variation in heat-transfer coefficient can be attributed entirely to the S/D effect since no Mach number variation was present.

In the cases discussed previously, the boundary layer was negligible, and in the present data the projection of the boundary-layer edge to the fin face intersected at an S/D around 1 or 2. In the data of Bushnell and Jones,[4] however, the projection of the boundary-layer edge to the fin leading edge intersected at an

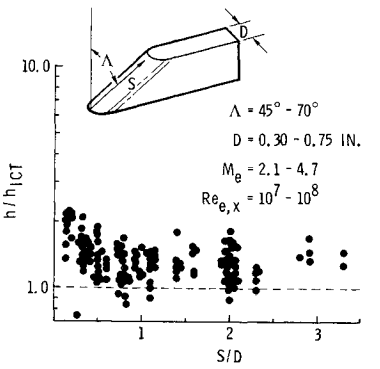

Fig. 11 Heat-transfer data as a function of nondimensional distance up the leading edge.

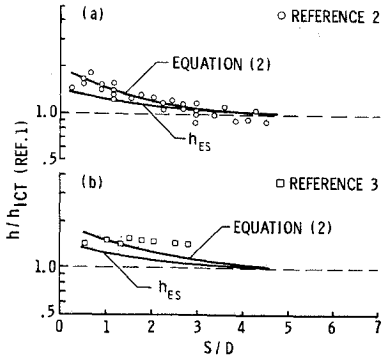

Fig. 12 Leading edge heat-transfer data of Beckwith[2] and Bushnell[3] compared with predictions.

S/D about 4 or 5—the region where end effects are dying out—and an entirely different trend is observed in the heat transfer data. In their experiment, a 69.45° swept fin with a cylindrical leading edge was immersed in the turbulent boundary layer on the wall of a wind-tunnel test section. Pressure- and heat-transfer data were obtained at a freestream Mach number of 6.15 and two Reynolds numbers. The heat-transfer data for the two Reynolds numbers are shown in Fig. 13 and compared with the predictions of ICT, the effective sweep method, and Eq. (2). For the lower Reynolds number, the values predicted using Eq. (2) give good agreement while the ICT predictions are well above the data and the effective sweep predictions even higher. The heat-transfer data at the higher Reynolds number approach a value somewhat lower than the expected theoretical value at large S/D and thus lie below all three predictions.

The data of Ref. 4 show that under certain conditions pressures greater than ICT values may be obtained while the heat transfer is less than the theoretical predictions. The effective sweep method does not predict such a reversal; however, the method proposed above [Eqs. (1) and (2)] predicts both the increase in pressure and decrease in heat transfer from the ICT values and gives reasonable agreement with the data.

This unexpected trend can be explained upon closer examination of the proposed prediction method and consideration of the sketch in Fig. 14. Assume that a fin is mounted on a sharp cone, a sharp wedge, or a tunnel wall so that the Mach number variation is entirely within the boundary layer. Also, assume the projection of the boundary layer intersects the fin leading edge at an S/D less than 5. Then the ICT values for pressure and heat

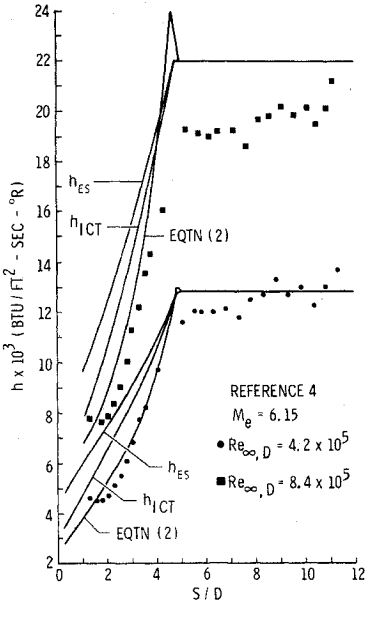

Fig. 13 Comparison of predictions with leading-edge heat-transfer data of Ref. 4.

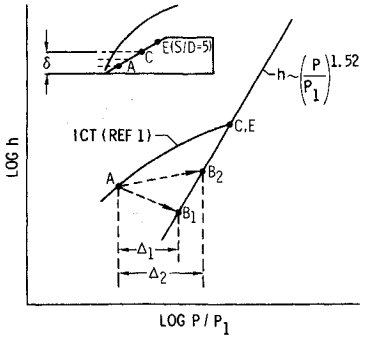

Fig. 14 Schematic of calculational method based on proposed prediction technique.

transfer increase as shown in the figure until the boundary-layer edge is reached (Point C), after which the theoretical values for all greater S/D are a constant. This value is also the point of intersection with the $h \sim (P/P_1)^{1.52}$ curve (Point E). For a given S/D a pressure rise and heat-transfer coefficient can be calculated using the strip method and ICT and plotted as Point A in the sketch. For this S/D, a dimensionless pressure increase due to end effects can be calculated using Eq. (1) rewritten in the form

$$\Delta = (P/P_1) - (P/P_1)_{ICT} = 0.65(P/P_1)_{ICT}\, e^{-(0.55S/D)}$$

The variation of Δ is difficult to assess intuitively without actual calculation due to its nonlinear dependence on flow conditions and geometry.

As shown in Fig. 14, the value of Δ is used to move from the theory curve to the $h \sim (P/P_1)^{1.52}$ curve. For a set of conditions such that $\Delta = \Delta_1$, the predicted value of h corresponds to Point B_1 and is less than the heat-transfer coefficient at Point A on the ICT curve. However, for flow conditions such that $\Delta = \Delta_2$, the predicted value is Point B_2 and is larger than the h predicted by ICT.

The leading-edge heat-transfer data of the present investigation nondimensionalized by the predictions of Eq. (2) are shown in Fig. 15 vs S/D. Agreement with prediction is on the order of the accuracy of the data.

Additional verification of the present technique was recently obtained when a 10° half-angle cone was flight tested at Mach numbers up to 4.3. The cone had two 60° swept fins mounted near the aft end with asymptotic calorimeters on the leading edges. Postflight fin heating calculations made using the technique were in excellent agreement with the flight data. Details of the flight and the data comparisons were reported in Ref. 12.

Summary

Analysis of the present data and those of others has shown that near the intersection of a leading edge and a vehicle a region exists in which the pressure and heat transfer cannot be

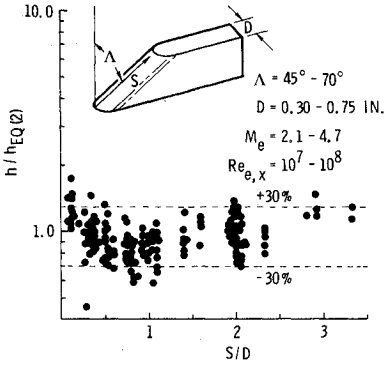

Fig. 15 Present leading-edge heat-transfer data nondimensionalized by predictions of the proposed technique vs nondimensional distance up the leading edge.

adequately predicted by theoretical approaches such as the turbulent theory of Beckwith and Gallagher for swept infinite cylinders. In this region, the curvature of the leading edge shock effectively decreases the sweep angle and leads to higher pressures than those predicted by ICT. However, the heat transfer to the leading edge can be either significantly above or below the ICT values, depending on the local flow conditions and geometry.

A technique has been developed for predicting leading-edge shock shapes, pressures, and turbulent heat transfer in this region. No prior knowledge of shock angles is required. Reasonable agreement with data was obtained for both cases where the heat transfer is greater than and less than ICT values. The data covered a range of $\Lambda = 45°$–$72°$, $M_e = 2.16$–7.33, and boundary-layer thicknesses intersecting the leading edge from $S/D \approx 0$ to 5.

The present pressure data indicate that the pressure increase over ICT values in the intersection region decreases with higher local Mach number. This is probably related to the behavior of the shock standoff distance, which exhibits a similar trend.

References

[1] Beckwith, I. E. and Gallagher, J. J., "Local Heat Transfer and Recovery Temperatures on a Yawed Cylinder at a Mach Number of 4.15 and High Reynolds Numbers," TR R-104, 1958, NASA.

[2] Beckwith, I. E., "Experimental Investigation of Heat Transfer and Pressures on a Swept Cylinder in the Vicinity of its Intersection with a Wedge and Flat Plate at Mach Number 4.15 and High Reynolds Numbers," TN D-2020, 1964, NASA.

[3] Bushnell, D. M., "Interference Heating on a Swept Cylinder in Region of Intersection with a Wedge at Mach Number 8," TN D-3094, 1965, NASA.

[4] Bushnell, D. M. and Jones, R. A., "Heat Transfer to a 70° Swept Fin Partially Submerged in a Turbulent Boundary Layer at Mach 6," TM X-1191, 1965, NASA.

[5] Coleman, H. W. and Lemmon, E. C., "Turbulent Heat Transfer and Pressure on Leading Edges of Fins Mounted on a Cone," SCL-RR-720308, 1972, Sandia Lab., Livermore, Calif.

[6] Coleman, H. W. and Lemmon, E. C., "Turbulent Heat Transfer and Pressure in the Interference Region of Fins Mounted on a Cone," SCL-RR-720309, 1973, Sandia Lab., Livermore, Calif.

[7] Lemmon, E. C. and Coleman, H. W., "Techniques for Reduction of Thin Skin Heat Transfer Data Containing Substantial Conduction Errors," SCL-RR-720310, 1973, Sandia Labs., Livermore, Calif.

[8] Arnold, J. W., *High Speed Wind Tunnel Facility Handbook,* Publication AER-E1R-13552-B, Feb. 1970, LTV Aerospace Corp., Vought Aeronautics Div., Dallas, Texas.

[9] Johnson, C. B. and Bushnell, D. M., "Power-Law Velocity-Profile-Exponent Variations with Reynolds Number, Wall Cooling, and Mach Number in a Turbulent Boundary Layer," TN D-5753, 1970, NASA.

[10] Martellucci, A., "Effect of Mass Transfer on Hypersonic Turbulent Boundary-Layer Properties," *AIAA Journal,* Vol. 10, No. 2, Feb. 1972, pp. 181–187.

[11] Eckstrom, D. J., "Engineering Analysis of Boundary Layer and Skin Friction on Bodies of Revolution at Zero Angle of Attack," LMSC/805162, AD 620 217, May 1965, Lockheed Missiles and Space Co., Sunnyvale, Calif.

[12] Lemmon, E. C. and Coleman, H. W., "Turbulent Heat Transfer to a Fin Leading Edge—Flight Test Results," *AIAA Journal,* Vol. 11, No. 4, April 1973, pp. 571–573.